THE JOURNAL OF PHYSICAL CHEMISTRY Letters

pubs.acs.org/JPCL Letter

Transient Depolarization Spectroscopic Study on Electronic Structure and Fluorescence Origin of Graphene Oxide

Yan Wang, Lei Wang,* Hai-Yu Wang,* Bing-Rong Gao, and Hong-Bo Sun

Cite This: *J. Phys. Chem. Lett.* 2020, 11, 1483−1489 Read Online

ACCESS | Metrics & More | Article Recommendations | Supporting Information

ABSTRACT: It is well-established that the electronic states of graphene oxide (GO) consist of sp^2 clusters with different sizes and the surrounding sp^3 matrix according to recent reports. However, addressing the excitation energy migration/redistribution among those electronic states in GO-based complex systems from spectroscopic experiments is still a challenge. Here, we combine the time-resolved absorption and fluorescence depolarization experiments to reveal the excitation energy migration processes in electronic states in GO. We demonstrate that, in sp^3 domains of GO, there are charge-transfer states between sp^3-hybridized carbon atoms and the oxygen-containing functional groups, and the energy redistribution and charge migration in sp^3 matrix occur on the time scale from subpicoseconds to tens of picoseconds. In contrast, the electronic states of sp^2 clusters in GO are rather localized and dominantly contribute to the excitation-wavelength-dependent red fluorescence of GO.

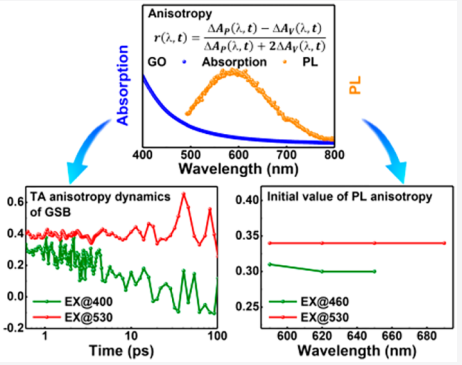

Since its discovery in 2004,[1] graphene as a carbon-based material has been applied in many scientific fields due to its exceptional mechanical strength and high electronic and thermal conductivities.[2−7] However, because of its hydrophobicity, its zero bandgap, and almost no emission, applications of graphene are limited in many optoelecctronic fields. Graphene oxide (GO) is a kind of two-dimensional material, which could be regarded as a "precursor" to produce graphene in a large-scale way.[8] In recent years, oxygen-containing functional groups have an extraordinary significance for GO. Those functional groups can link GO with other metals or nonmetallic nanoparticles by noncovalent or covalent chemical bonds, creating a series of excellent optical and electrical properties for GO-based nanocomposites.[9−19] However, due to the lack of deep understanding of the electronic structure of GO, it still has been a challenge to improve the performance of these nanocomposites. For instance, one of crucial controversies is that the fluorescence origin of GO has not yet been fully determined. In addition, this issue has a great influence on the optoelecctronic properties of those GO-based complex systems. Hence, in order to improve the performance of GO-based nanocomposites and increase the application fields of GO, a comprehensive understanding on the electronic structure of GO is of great significance.

The study of the structure of GO has been carried out, and some useful information about the electronic structure of GO is obtained by means of various spectroscopic techniques such as Raman and X-ray-based spectroscopies,[20−25] and other characterization methods, like scanning tunneling microscopy and atomic force microscopy.[26] From those techniques, it has been noted that GO possesses local sp^2 domains, which are also randomly distributed on GO with a high carrier transport mobility. Moreover, GO contains an sp^3 matrix, mainly caused by the oxygen-containing functional groups. As a result, GO is a naturally inhomogeneous system which is constituted of complex electronic states. Time-resolved spectroscopic experiments are the most direct ways to understand the electronic structure evolution and carrier relaxation after the photon excitation. In our previous work, by selective excitations on electronic states of GO, not only are sp^2 clusters and the sp^3 matrix clearly distinguished, but also these directly indicated the sp^2 domains with different sizes (mostly like transient spectral hole-burning experiments).[27] Furthermore, we also observed insulator−semiconductor−semimetal transitions in GO, which correspond to less and less oxygen content for the GO samples.[28]

To further reveal the relationship between various electronic states in GO, we need to know how the excitation energy migrates/redistributes among those electronic states in GO-based complex systems. It is worth noting that the energy redistribution also means the electronic excitations are jumping among various states, which will cause a random change in the direction of a transition dipole moment, and, subsequently, a loss of the spectral anisotropy. Thus, transient depolarization experiments are suggested to measure the energy redistribution and relaxation in an inhomogeneous electronic system through

Received: December 6, 2019
Accepted: February 4, 2020
Published: February 4, 2020

https://dx.doi.org/10.1021/acs.jpclett.9b03613
J. Phys. Chem. Lett. 2020, 11, 1483−1489

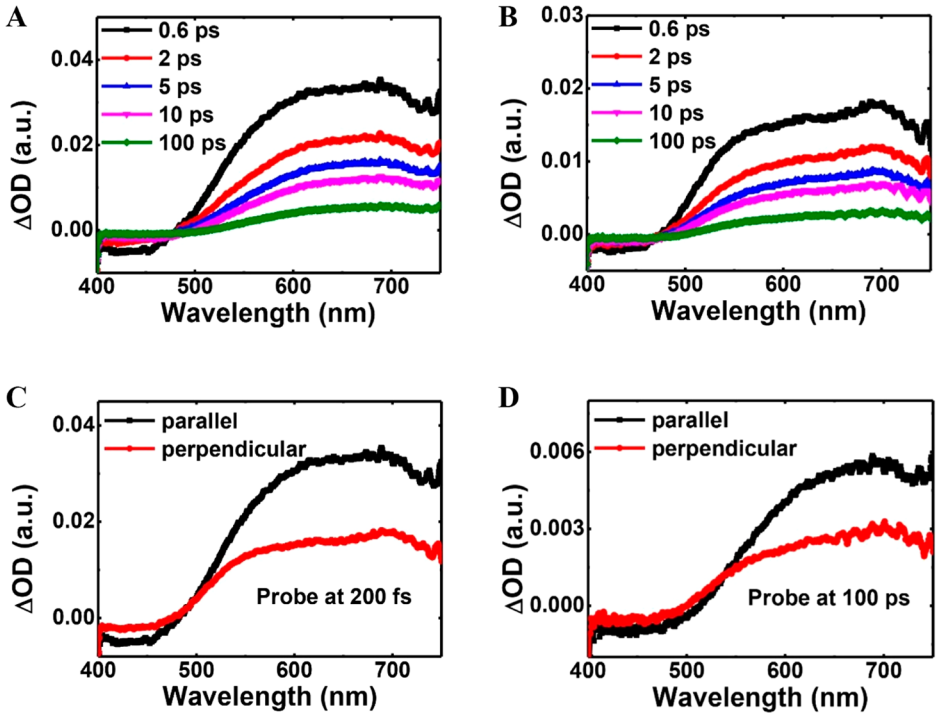

Figure 1. (A) Parallel transient absorption spectra of GO under 400 nm excitation. (B) Perpendicular transient absorption spectra of GO under 400 nm excitation. (C) A comparison between parallel and perpendicular spectra for GO at 200 fs. (D) A comparison between parallel and perpendicular spectra for GO at 100 ps.

monitoring the fluorescence or through absorption anisotropy decay. In fact, the fluorescence anisotropy experiments were carried out in GO, where a considerable energy redistribution was observed on the subpicoseconds to tens of picoseconds time scale.[29] However, its energy migration experimental results, which are only pumped at 400 nm, cannot correspond to more exact electronic states. In this paper, we combine transient absorption and time-resolved fluorescence depolarization experiments to measure the anisotropy decay of special electronic states (such as sp^2 domains and sp^3 region) in GO, by a selective excitation approach. The relationship between those electronic states and the origin of red fluorescence in GO is discussed.

In the experiment, we make the polarization direction of pump and probe lights parallel at first to get a transient absorption spectrum, called a parallel spectrum, $\Delta A_p(\lambda, t)$. Then, we change the polarization direction of probe light perpendicularly to that of the pump light, and get a perpendicular spectrum, $\Delta A_v(\lambda, t)$. Thus, the anisotropy value of different wavelengths, $r(\lambda, t)$, can be calculated using eq 1.

$$r(\lambda, t) = \frac{\Delta A_p(\lambda, t) - \Delta A_v(\lambda, t)}{\Delta A_p(\lambda, t) + 2\Delta A_v(\lambda, t)} \quad (1)$$

The maximum and minimum values of anisotropy are 0.4 and −0.2, respectively, which correspond to the directions of transition dipolar moment parallel and perpendicular to that of excitation. In general, the rotational diffusion also will cause the anisotropy loss; however, the time constant for this process is far away from the time scale we are concerned about, because of the large size of GO (usually on the hundreds of nanometers to micrometers scale). So, the anisotropy decay will simply reflect the electronic excitation or charge migrating between various states in GO. Experimental methods and the photophysical model of GO are presented in the Supporting Information.

First, we use a 400 nm laser to selectively excite the sp^3 matrix in GO in transient absorption experiments. The parallel and perpendicular transient absorption spectra of GO are displayed in Figure 1A,B, respectively. As previous reports indicate, the negative signals ranging from 400 to 475 nm are corresponding to the ground-state bleaching of the sp^3 electronic states (or so-called hybrid states) in GO, and the broad positive signals starting from 475 to 750 nm are the excited-state absorption signals caused by the oxygen-containing functional groups, since the amplitude of these positive signals significantly decreases as the amount of oxygen-containing species becomes less and less.[27,28]

The parallel and perpendicular transient absorption spectra at the same probe time can be put together, and the difference of signal amplitude at each wavelength clearly shows the relative anisotropy, which remains from the initial time (~200 fs, Figure 1C) to even 100 ps (Figure 1D) after pump light excitation. In a comparison with fluorescence anisotropy, the analysis of transient absorption anisotropy is usually more complicated. Because the signal in some spectral ranges combines the contribution of multitransitions (such as ground-state bleaching and excited-state absorption), the calculated anisotropy values are unreasonable sometimes. Figure S1 shows the calculated initial (about 200 fs) anisotropy spectrum, in which, for convenience, the anisotropy values in transient absorption experiments are performed as $\Delta A_p/\Delta A_v$ (it should be between 3 and 1/2, which corresponds to the value of r between 0.4 and −0.2). In the spectral range from 470 to 480 nm in Figure S1, there is an extremely large anisotropy value due to the overlap of ground-state bleaching and absorption of the oxygen-containing functional groups (a crossing point of transient spectral signals). Fortunately, for the main part of the ground-state bleaching

https://dx.doi.org/10.1021/acs.jpclett.9b03613
J. Phys. Chem. Lett. 2020, 11, 1483−1489

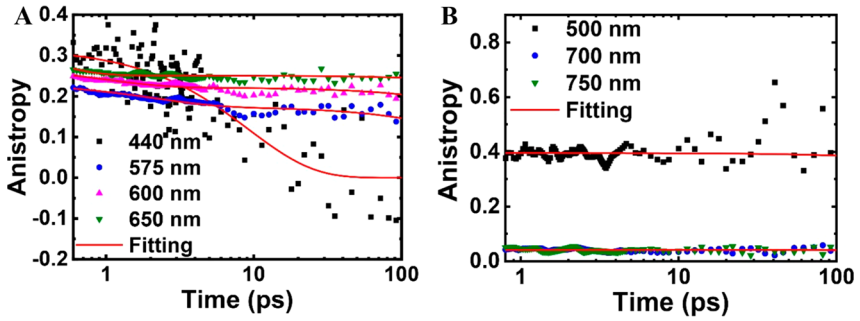

Figure 2. (A) Transient absorption anisotropy kinetics of GO at 440, 575, 600, and 650 nm under 400 nm excitation. (B) Transient absorption spectra anisotropy kinetics of GO at 500, 700, and 750 nm under 530 nm excitation.

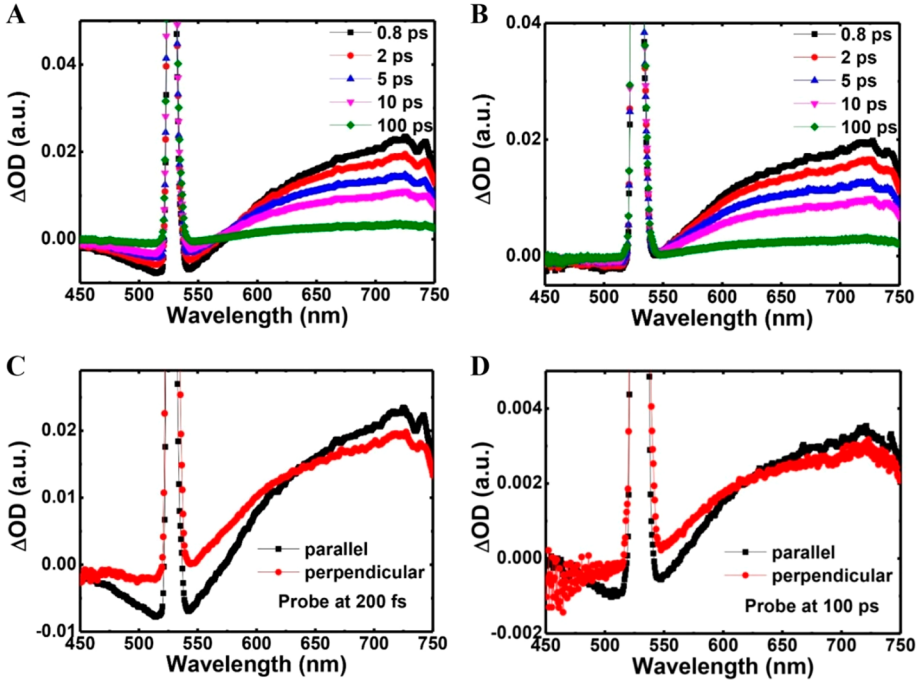

Figure 3. (A) Parallel transient absorption spectra of GO under 530 nm excitation. (B) Perpendicular transient absorption spectra of GO under 530 nm excitation. (C) A comparison between parallel and perpendicular spectra for GO at 200 fs. (D) A comparison between parallel and perpendicular spectra for GO at 100 ps.

signal in the range 400−470 nm in Figure S1, the anisotropy retains the same value of 2.2 ± 0.3 (corresponding to $r = 0.29 \pm 0.05$) that indicates a perfect single-transition contribution. For the wavelengths longer than 480 nm in Figure S1, there are reasonable anisotropy values, where the variety of anisotropy values at different wavelengths may be partly due to the contributions of different oxygen-containing functional groups.

As mentioned before for GO, the anisotropy decay on the time scale we examined will be mainly affected by the excitation energy migration/redistribution processes. First, the ground-state bleaching part under 400 nm excitation reflects the situation of the sp^3 electronic state, in which the large initial value of anisotropy indicates that the direction of transition dipole moment slightly changes after the pump light excitation. We choose the anisotropy kinetics at 440 nm ($r = 0.33 \pm 0.01$) to represent the case of excited sp^3 domains (as shown in Figure 2A, the original dynamics of parallel and perpendicular signals are shown in Figure S2). On the basis of the best-fit parameters of transient absorption anisotropy kinetic curves of GO with a function $I \propto \Sigma_i A_i \exp(-t/\tau_i)$ presented in Table S1, this anisotropy kinetics for the ground-state bleaching part exhibits single-exponential decay behavior with a lifetime of 9.3 ± 1.4 ps, which indicates there could be a dominant energy migration approach in sp^3 domains.

For the excited-state absorption part under 400 nm excitation, the initial values of represented anisotropy kinetics at 575, 600, and 650 nm are 0.22 ± 0.01, 0.25 ± 0.01, and 0.26 ± 0.01, respectively, as shown in Figure 2A. It is interesting that, different from the anisotropy decay dynamics of the ground-state bleaching part, considerable anisotropy (more than 70% of initial anisotropy values) remains even at 100 ps after pump light excitation for the excited-state absorption part under 400 nm excitation. Our fitting parameters also indicate that all three wavelengths have two decay lifetimes for the anisotropy kinetics. For the probed wavelength at 575 nm, the fitted lifetime is 2.1 ± 0.3 ps (25%) and 563 ± 27 ps (75%), respectively. For the probed wavelength at 600 nm, the fitted lifetime is 0.95 ± 0.14 ps (19%) and 1230 ± 45 ps (81%), respectively. For the probed wavelength at 650 nm, the fitted lifetime is 0.27 ± 0.02 ps (37%) and 4693 ± 275 ps (63%), respectively. In the parentheses are the relative weights for the fitted lifetimes. As a result, the longer probe wavelength has a longer average lifetime from hundreds of

https://dx.doi.org/10.1021/acs.jpclett.9b03613
J. Phys. Chem. Lett. 2020, 11, 1483−1489

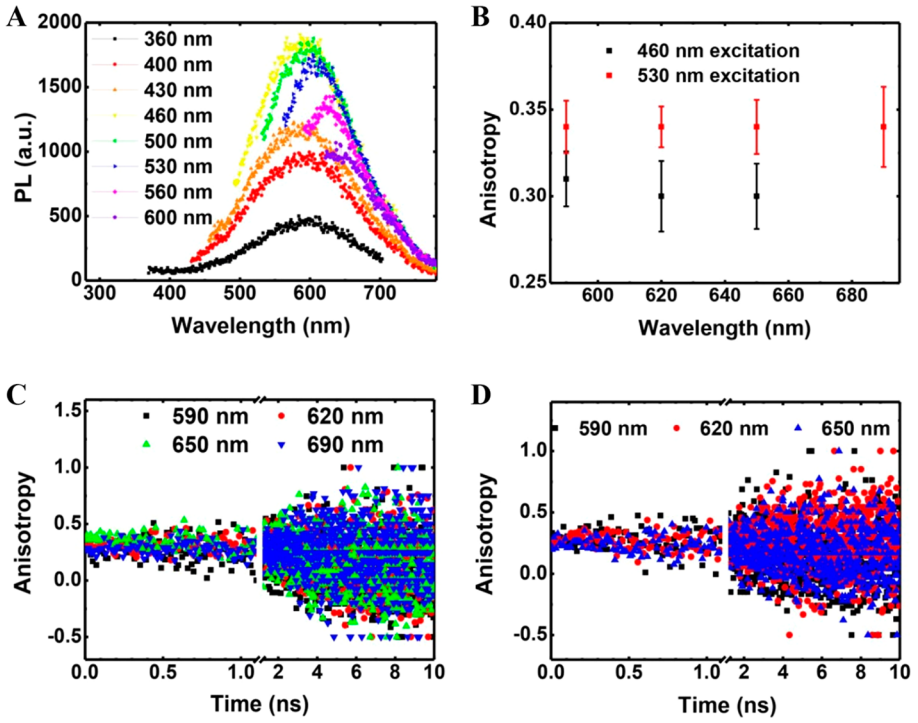

Figure 4. (A) Steady-state emission spectra of GO under different excitation wavelengths. (B) Initial values of time-resolved fluorescence anisotropy at different detection wavelengths under 460 and 530 nm excitations. (C) Time-resolved fluorescence anisotropy traces of GO at 590, 620, 650, and 690 nm under 530 nm excitation. (D) Time-resolved fluorescence anisotropy traces of GO at 590, 620, and 650 nm under 460 nm excitation.

picoseconds to several nanoseconds for the anisotropy decay, as shown in Table S1.

In fact, sp^3-hybridized carbon atoms and the linked oxygen-containing functional groups construct the electronic system of sp^3 domains, including the peripheral part (close to sp^2 domains) and the inside part. If the photogenerated electrons and holes in sp^3 domains are tightly bound together as a whole, the anisotropy kinetics of both ground-state bleaching and excited-state absorption parts will follow the same decay process. However, our transient absorption depolarization experimental results do not support this hypothesis. One reason could be that those electrons and holes are separated to form the so-called charge-transfer states between sp^3-hybridized carbon atoms and oxygen-containing functional groups. Hence, such a large anisotropy loss of the ground-state bleaching part under 400 nm excitation within the first 100 ps should be mainly due to the electron or hole jumping among sp^3-hybridized carbon atoms at different locations, toward the nearest peripheral part of the sp^3 domains. This may explain why GO can be efficiently reduced by UV light, because those charge-transfer states could be helpful for the desorption of oxygen-containing functional groups.[30] While there is not an efficient charge migration for the relevant excited-state absorption part, because its anisotropy still remains substantial within the same time scale. Another possible reason which could cause the anisotropy dynamics difference between negative ground-state bleaching and positive excited-state absorption parts is that this positive signal may partly contain the contributions of excited sp^2 clusters (the anisotropy of sp^2 clusters will almost remain constant for hundreds of picoseconds, see Figure 2B). Why can sp^2 clusters be excited when we pump the sp^3 region? In our previous work, it was observed that a ground bleaching signal around 420 nm, which can extend to the wavelength range shorter than 400 nm, was always accompanied by the excitation of sp^2 clusters (selective excitation by pump lights).[27] This implies that this high energy state shares the same ground state with the sp^2 clusters, because it is common for all sp^2 clusters with various sizes. Thus, it can also be considered as one kind of higher electronic state (hybrid states) for sp^2 clusters in GO, resulting from the interaction between the edge of the sp^2 clusters and the peripheral part of the sp^3 matrix. Therefore, under 400 nm laser pumping, a small amount of these hybrid states would be excited and then quickly relax to the first excited state of sp^2 clusters, which could lead to a loss for the initial anisotropy value of the excited-state absorption part. Clearly, this is a minor contribution to the initial anisotropy values of the excited-state absorption part in the range 575−650 nm, compared to that under 530 nm excitation (Figure 2B).

Next, for sp^2 clusters, we select a 530 nm laser to excite GO in the experiment. The parallel and perpendicular transient absorption spectra of GO are shown in Figure 3. For the parallel spectrum under 530 nm excitation (Figure 3A), we can observe a clear ground-state bleaching signal from 450 to 575 nm, of which the center position coincides with the excitation wavelength, indicating the selective excitation effect corresponding to sp^2 clusters with a certain size.[27] In the perpendicular spectrum under 530 nm excitation (Figure 3B), the ground-state bleaching signal is much smaller (the same trend as the 400 nm excitation case), so a large anisotropy is expected for this sp^2 excitation. Similar to the sp^3 excitation (400 nm pumping) case, both the parallel and perpendicular transient absorption spectra under 530 nm excitation also show large excited-state absorption signals, relative to oxygen-containing functional groups around the sp^2 clusters. However, the amplitude differences of the excited-state absorption part under 530 nm excitation are much smaller than that under 400 nm excitation, as shown in Figure 3C,D, implying a very low initial anisotropy value. In order to avoid the disturbance of pump lights and the overlapping of

https://dx.doi.org/10.1021/acs.jpclett.9b03613
J. Phys. Chem. Lett. 2020, 11, 1483−1489

ground-state bleaching and excited-state absorption signals, we choose the bleaching signal at 500 nm to represent the ground-state bleaching part, and the signals at 700 and 750 nm to represent the excited-state absorption part, respectively. Thus, when we calculate anisotropy kinetics, those signals are far enough away from the possible signal mixing zone (550−650 nm) (the original dynamics of parallel and perpendicular signals under 530 nm excitation are shown in Figure S3). The initial anisotropy at 500 nm has an ideal maximum value of 0.40 ± 0.01. This indicates that the observed bleaching state is exactly the state created by the excitation light, and this value also remains well in the first 100 ps (Figure 2B). This means the electronic excitation is completely localized at the sp^2 clusters, and the electron−hole pairs are tightly binding together. This also indicates that the excitation energy cannot transfer to other larger sp^2 clusters and the surrounding sp^3 matrix. For the excited-state absorption part under 530 nm excitation, the initial values of anisotropy at 700 and 750 nm are almost the same as about 0.04 ± 0.01 (the small anisotropy may be due to a large change of the direction of the dipole moment for the excited-state absorption processes), and their values also remain within the 100 ps probe window as shown in Figure 2B. Our fitting results for the anisotropy kinetics under 530 excitation confirm it is a nanosecond time scale decay process (Table S1). Those convincing pieces of evidence demonstrate that when the sp^2 clusters are directly excited, energy or charge migration does not occur.

Then, we have to answer the question of where the energy/charge could finally transfer. As we know, GO usually has a weak and broadband fluorescence, covering spectral regions from UV to near-infrared as reported in the literature.[30,31] So, one of the destinies for the energy/charge is probably radiative recombination. In other words, we want to know which electronic state could be responsible for the main part of fluorescence of GO. For the origin of the blue fluorescence, it could be mainly attributed to quasimolecules on the GO linked by oxygen-containing functional groups.[29,32−34] However, for the red fluorescence of GO, its origin is still a controversial issue.[29,35−37] Figure 4A shows the steady-state fluorescence of GO in our experiments under different pump lights from 360 to 600 nm. A broad emission band appears for GO from 400 to 750 nm. When the pump light changes from 360 to 460 nm, the fluorescence peak of GO is fixed at 590 nm. When the excitation wavelength changes from 500 to 600 nm, the fluorescence peak of GO shows a continuous redshift from 590 to 650 nm. This excitation-wavelength-dependent fluorescence property is consistent with previous reports.[37]

Time-resolved fluorescence depolarization experiments are carried out to investigate the origin of red emission in GO. Time-resolved fluorescence experiments are based on the time-correlated single-photon counting (TCSPC) system; the time constant of the instrument response function is about 200 ps.[38] In order to compare with the transient absorption experimental results, we choose the excitation wavelengths at 530 and 460 nm for the fluorescence anisotropy experiments. The initial fluorescence anisotropy values are shown in Figure 4B. Under 530 nm excitation, the initial fluorescence anisotropy values probed at 590, 620, 650, and 690 nm have the same initial value at 0.34 ± 0.02, which nearly does not decay even to 10 ns (Figure 4C; the original fluorescence dynamics under parallel and perpendicular excitations are shown in Figure S4). This is consistent with results of a transient absorption depolarization experiment under 530 nm excitation, and it indicates that the red fluorescence of GO has a dominant contribution from the sp^2 clusters with a very localized electronic state around 2.34 eV (530 nm). For the fluorescence anisotropy experiment under 460 nm excitation, the initial fluorescence anisotropy values probed at 590, 630, and 650 nm also have a considerable initial value at 0.30 ± 0.02 and maintain 10 ns time scales, too (Figure 4D; the original fluorescence dynamics under parallel and perpendicular excitations are shown in Figure S5). The slightly smaller initial fluorescence anisotropy values under 460 nm excitation may be caused by the excitation energy closer to the sp^3 domains.

In conclusion, we have combined the transient absorption and fluorescence depolarization experiments to investigate the excitation energy migration processes in electronic states in GO. The anisotropy signals are clearly distinguished for both sp^3 and sp^2 excitations. In the sp^3 domain of GO, a kind of charge-transfer state exists between sp^3-hybridized carbon atoms and the oxygen-containing functional groups; the energy redistribution and charge migration in an sp^3 matrix occur from subpicoseconds to tens of picoseconds. The sp^2 clusters in GO have a very localized electronic state and dominantly contribute to the red fluorescence of GO sheets. Hence, for the steady-state fluorescence of GO, the fluorescence peak position (590−650 nm) could be decided by the average size of sp^2 clusters in each GO sample; the redshift feature of the fluorescence peak under different pump lights (500−600 nm) is due to the selective excitation of the sp^2 clusters with a larger size, where the corresponding fluorescence intensities are amplified. Our findings provide a comprehensive picture for understanding the electronic states and related florescence properties in GO. The results can also explain the origin of the near-infrared fluorescence of GO revealed by time-resolved fluorescence experiments.[36] That is, their GO sample has a near-infrared fluorescence peak at about 730 nm (~1.7 eV), corresponding to a relatively larger average size of sp^2 clusters and probably a closer distance between the different sp^2 clusters, which favors the completion of the energy transfer under a UV excitation condition. We believe that there are still abundant physical processes in various GO samples (such as changing the size, oxygen content, and surrounding environment), which are worth further studying to better understand the photophysical properties of GO by the transient depolarization techniques.

■ ASSOCIATED CONTENT

Supporting Information

The Supporting Information is available free of charge at https://pubs.acs.org/doi/10.1021/acs.jpclett.9b03613.

Experimental details, calculated initial anisotropy spectrum (at 200 fs) under 400 nm excitation, and parallel and perpendicular transient absorption/time-resolved fluorescence decay curves of GO (PDF)

■ AUTHOR INFORMATION

Corresponding Authors

Lei Wang − *State Key Laboratory of Integrated Optoelectronics, College of Electronic Science and Engineering, Jilin University, Changchun 130012, China;* orcid.org/0000-0003-4304-2887; Phone: + 81-431-8516-8281; Email: lei_wang@jlu.edu.cn; Fax: + 81-431-8516-8270

Hai-Yu Wang − *State Key Laboratory of Integrated Optoelectronics, College of Electronic Science and Engineering, Jilin University, Changchun 130012, China*; Phone: + 81-431-

https://dx.doi.org/10.1021/acs.jpclett.9b03613
J. Phys. Chem. Lett. 2020, 11, 1483−1489

8516-8281; Email: haiyu_wang@jlu.edu.cn; Fax: + 81-431-8516-8270

Authors

Yan Wang − *State Key Laboratory of Integrated Optoelectronics, College of Electronic Science and Engineering, Jilin University, Changchun 130012, China*

Bing-Rong Gao − *State Key Laboratory of Integrated Optoelectronics, College of Electronic Science and Engineering, Jilin University, Changchun 130012, China*

Hong-Bo Sun − *State Key Laboratory of Integrated Optoelectronics, College of Electronic Science and Engineering, Jilin University, Changchun 130012, China; State Key Laboratory of Precision Measurement Technology and Instruments, Department of Precision Instrument, Tsinghua University, Haidian, Beijing 100084, China;* orcid.org/0000-0003-2127-8610

Complete contact information is available at: https://pubs.acs.org/10.1021/acs.jpclett.9b03613

Author Contributions

The manuscript was written through contributions of all authors. All authors have given approval to the final version of the manuscript.

Notes

The authors declare no competing financial interest.

■ ACKNOWLEDGMENTS

This work was supported by the National Key Research and Development Program of China and the National Natural Science Foundation of China (NSFC) under Grants 2017YFB1104600, 21773087, 21603083, 61590930, and 21473077, as well as by the China Postdoctoral Science Foundation (2016M590259).

■ REFERENCES

(1) Novoselov, K. S.; Geim, A. K.; Morozov, S. V.; Jiang, D.; Zhang, Y.; Dubonos, S. V.; Grigorieva, I. V.; Firsov, A. A. Electric Field Effect in Atomically Thin Carbon Films. *Science* **2004**, *306*, 666−669.

(2) Geim, A. K.; Novoselov, K. S. The Rise of Graphene. *Nat. Mater.* **2007**, *6*, 183−191.

(3) Lee, C.; Wei, X.; Kysar, J. W.; Hone, J. Measurement of the Elastic Properties and Intrinsic Strength of Monolayer Graphene. *Science* **2008**, *321*, 385−388.

(4) Bolotin, K. I.; Sikes, K. J.; Jiang, Z.; Klima, M.; Fudenberg, G.; Hone, J.; Kim, P.; Stormer, H. L. Ultrahigh Electron Mobility in Suspended Graphene. *Solid State Commun.* **2008**, *146*, 351−355.

(5) Zhang, Y.; Tan, Y. W.; Stormer, H. L.; Kim, P. Experimental Observation of the Quantum Hall Effect and Berry's Phase in Graphene. *Nature* **2005**, *438*, 201−204.

(6) Geim, A. K. Graphene: Status and Prospects. *Science* **2009**, *324*, 1530−1534.

(7) Wang, X.; Zhi, L. J.; Müllen, K. Transparent, Conductive Graphene Electrodes for Dye-Sensitized Solar Cells. *Nano Lett.* **2008**, *8*, 323−327.

(8) Gilje, S.; Han, S.; Wang, M. S.; Wang, K. L.; Kaner, R. B. A Chemical Route to Graphene for Device Applications. *Nano Lett.* **2007**, *7*, 3394−3398.

(9) Bissessur, R.; Scully, S. F. Intercalation of Solid Polymer Electrolytes into Graphite Oxide. *Solid State Ionics* **2007**, *178*, 877−882.

(10) Compton, O. C.; Nguyen, S. T. Graphene Oxide, Highly Reduced Graphene Oxide, and Graphene: Versatile Building Blocks for Carbon-Based Materials. *Small* **2010**, *6*, 711−723.

(11) Park, S.; Ruoff, R. S. Chemical Methods for the Production of Graphenes. *Nat. Nanotechnol.* **2009**, *4*, 217−224.

(12) Zhang, X. Y.; Sun, S. H.; Sun, X. J.; Zhao, Y. R.; Chen, L.; Yang, Y.; Lu, W.; Li, D. B. Plasma-Induced, Nitrogen-Doped Graphene-Based Aerogels for High-Performance Supercapacitors. *Light: Sci. Appl.* **2016**, *5*, No. e16130.

(13) Wu, Y. H.; Luo, Y.; Qu, J. K.; Daoud, W. A.; Qi, T. Liquid Single-Electrode Triboelectric Nanogenerator Based on Graphene Oxide Dispersion for Wearable Electronics. *Nano Energy* **2019**, *64*, 103948.

(14) Li, Y. J.; Gao, W.; Ci, L. J.; Wang, C. M.; Ajayan, P. M. Catalytic Performance of Pt Nanoparticles on Reduced Graphene Oxide for Methanol Electro-Oxidation. *Carbon* **2010**, *48*, 1124−1130.

(15) Yin, Z. Y.; Wu, S. X.; Zhou, X. Z.; Huang, X.; Zhang, Q. C.; Boey, F.; Zhang, H. Electrochemical Deposition of ZnO Nanorods on Transparent Reduced Graphene Oxide Electrodes for Hybrid Solar Cells. *Small* **2010**, *6*, 307−312.

(16) Yang, W.; Chata, G.; Zhang, Y. D.; Peng, Y.; Lu, J. E.; Wang, N.; Mercado, R.; Li, J.; Chen, S. W. Graphene Oxide-Supported Zinc Cobalt Oxides as Effective Cathode Catalysts for Microbial Fuel Cell: High Catalytic Activity and Inhibition of Biofilm Formation. *Nano Energy* **2019**, *57*, 811−819.

(17) Chong, S. K.; Sun, L.; Shu, C. Y.; Guo, S. W.; Liu, Y. N.; Wang, W.; Liu, H. K. Chemical Bonding Boosts Nano-Rose-Like MoS2 Anchored on Reduced Graphene Oxide for Superior Potassium-Ion Storage. *Nano Energy* **2019**, *63*, 103868.

(18) Dong, L. F.; Gari, R. R. S.; Li, Z.; Craig, M. M.; Hou, S. F. Graphene-Supported Platinum and Platinum-Ruthenium Nanoparticles with High Electrocatalytic Activity for Methanol and Ethanol Oxidation. *Carbon* **2010**, *48*, 781−787.

(19) Paek, S. M.; Yoo, E.; Honma, I. Enhanced Cyclic Performance and Lithium Storage Capacity of SnO_2/Graphene Nanoporous Electrodes with Three-Dimensionally Delaminated Flexible Structure. *Nano Lett.* **2009**, *9*, 72−75.

(20) Gómez-Navarro, C.; Weitz, R. T.; Bittner, A. M.; Scolari, M.; Mews, A.; Burghard, M.; Kern, K. Electronic Transport Properties of Individual Chemically Reduced Graphene Oxide Sheets. *Nano Lett.* **2007**, *7*, 3499−3503.

(21) Kudin, K. N.; Ozbas, B.; Schniepp, H. C.; Prud'homme, R. K.; Aksay, I. A.; Car, R. Raman Spectra of Graphite Oxide and Functionalized Graphene Sheets. *Nano Lett.* **2008**, *8*, 36−41.

(22) Lee, V.; Whittaker, L.; Jaye, C.; Baroudi, K. M.; Fischer, D. A.; Banerjee, S. Large-Area Chemically Modified Graphene Films: Electrophoretic Deposition and Characterization by Soft X-ray Absorption Spectroscopy. *Chem. Mater.* **2009**, *21*, 3905−3916.

(23) Lee, D. W.; De Los Santos V., L.; Seo, J. W.; Felix, L. L.; Bustamante D., A.; Cole, J. M.; Barnes, C. H. W. The Structure of Graphite Oxide: Investigation of Its Surface Chemical Groups. *J. Phys. Chem. B* **2010**, *114*, 5723−2728.

(24) Ganguly, A.; Sharma, S.; Papakonstantinou, P.; Hamilton, J. Probing the Thermal Deoxygenation of Graphene Oxide Using High-Resolution In Situ X-ray-Based Spectroscopies. *J. Phys. Chem. C* **2011**, *115*, 17009−17019.

(25) Zhang, W. H.; Carravetta, V.; Li, Z. Y.; Luo, Y.; Yang, J. L. Oxidation States of Graphene: Insights from Computational Spectroscopy. *J. Chem. Phys.* **2009**, *131*, 244505.

(26) Paredes, J. I.; Villar-Rodil, S.; Solís-Fernández, P.; Martínez-Alonso, A.; Tascón, J. M. D. Atomic Force and Scanning Tunneling Microscopy Imaging of Graphene Nanosheets Derived from Graphite Oxide. *Langmuir* **2009**, *25*, 5957−5968.

(27) Wang, L.; Wang, H. Y.; Wang, Y.; Zhu, S. J.; Zhang, Y. L.; Zhang, J. H.; Chen, Q. D.; Han, W.; Xu, H. L.; Yang, B.; Sun, H. B. Direct Observation of Quantum Confined Graphene Like States and Novel Hybrid States in Graphene Oxide by Transient Spectroscopy. *Adv. Mater.* **2013**, *25*, 6539−6545.

(28) Wang, Y.; Wang, L.; Wang, H. Y.; Chen, Q. D.; Sun, H. B. Ultrafast Spectroscopic Study of Insulator-Semiconductor-Semimetal Transitions in Graphene Oxide and Its Reduced Derivatives. *J. Phys. Chem. C* **2019**, *123*, 22550−22555.

(29) Exarhos, A. L.; Turk, M. E.; Kikkawa, J. M. Ultrafast Spectral Migration of Photoluminescence in Graphene Oxide. *Nano Lett.* **2013**, *13*, 344−349.

(30) Yue, Y. Y.; Chen, Y.; Zhang, Y. X.; Wang, L.; Wang, H. Y. Fluorescence Evolution Processes of Visible/Ultraviolet Photo-reduced Graphene Oxide. *Opt. Mater. Express* **2017**, *7*, 2519−2527.
(31) Kozawa, D.; Miyauchi, Y.; Mouri, S.; Matsuda, K. Changing Photoluminescence Spectra of Graphene Oxide by Centrifugation Treatments. *Phys. Status Solidi C* **2013**, *10*, 1600−1603.
(32) Kozawa, D.; Miyauchi, Y.; Mouri, S.; Matsuda, K. Exploring the Origin of Blue and Ultraviolet Fluorescence in Graphene Oxide. *J. Phys. Chem. Lett.* **2013**, *4*, 2035−2040.
(33) Konkena, B.; Vasudevan, S. Spectral Migration of Fluorescence in Graphene Oxide Aqueous Dispersions: Evidence for Excited-State Proton Transfer. *J. Phys. Chem. Lett.* **2014**, *5*, 1−7.
(34) Galande, C.; Mohite, A. D.; Naumov, A. V.; Gao, W.; Ci, L. J.; Ajayan, A.; Gao, H.; Srivastava, A.; Weisman, R. B.; Ajayan, P. M. Quasi-Molecular Fluorescence from Graphene Oxide. *Sci. Rep.* **2011**, *1*, 85.
(35) Cushing, S. K.; Li, M.; Huang, F.; Wu, N. Q. Origin of Strong Excitation Wavelength Dependent Fluorescence of Graphene Oxide. *ACS Nano* **2014**, *8*, 1002−1013.
(36) Kozawa, D.; Zhu, X.; Miyauchi, Y.; Mouri, S.; Ichida, M.; Su, H. B.; Matsuda, K. Excitonic Photoluminescence from Nanodisc States in Graphene Oxides. *J. Phys. Chem. Lett.* **2014**, *5*, 1754−1759.
(37) Shang, J.; Ma, L.; Li, J. W.; Ai, W.; Yu, T.; Gurzadyan, G. G. The Origin of Fluorescence from Graphene Oxide. *Sci. Rep.* **2012**, *2*, 792.
(38) Hao, Y. W.; Wang, H. Y.; Zhang, Z. Y.; Zhang, X. L.; Chen, Q. D.; Sun, H. B. Time-Resolved Fluorescence Anisotropy of Surface Plasmon Coupled Emission on Metallic Gratings. *J. Phys. Chem. C* **2013**, *117*, 26734−26739.

https://dx.doi.org/10.1021/acs.jpclett.9b03613
J. Phys. Chem. Lett. 2020, 11, 1483−1489